Radiotherapy and Oncology 201 (2024) 110539

Contents lists available at ScienceDirect

Radiotherapy and Oncology

journal homepage: www.thegreenjournal.com

Original Article

In vivo measurements of change in tissue oxygen level during irradiation reveal novel dose rate dependence

Veljko Grilj [a,b,1,*], Ron J. Leavitt [b,1], Mirna El Khatib [c,d], Ryan Paisley [a], Javier Franco-Perez [b,e,g], Benoit Petit [b,f,g], Paola Ballesteros-Zebadua [b,e,g], Marie-Catherine Vozenin [b,f,g]

[a] *Institute of Radiation Physics, University Hospital and University of Lausanne, Lausanne, Switzerland*
[b] *Radiation Oncology Laboratory, Department of Radiation Oncology, Lausanne, University Hospital and University of Lausanne, Lausanne, Switzerland*
[c] *Department of Biochemistry and Biophysics, Perelman School of Medicine, University of Pennsylvania, Philadelphia, PA, United States*
[d] *Department of Chemistry, School of Arts and Sciences, University of Pennsylvania, Philadelphia, PA, United States*
[e] *Instituto Nacional de Neurología y Neurocirugía Manuel Velasco Suarez, Mexico City, Mexico*
[f] *Radiotherapy and Radiobiology Sector, Radiation Therapy Service, University Hospital of Geneva, Geneva, Switzerland*
[g] *LiRR- Laboratory of Innovation in Radiobiology Applied to Radiotherapy, Faculty of Medicine, University of Geneva, Geneva, Switzerland*

A B S T R A C T

Background and purpose: This study aimed to investigate the radiochemical oxygen depletion (ROD) *in vivo* by directly measuring oxygen levels in various mouse tissues during ultra-high dose rate (UHDR) irradiation at clinically relevant doses and dose rates.
Materials and methods: Mice bearing subcutaneous human glioblastoma (U-87 MG) tumors were used for tumor and normal tissue (skin, muscle, brain) measurements. An oxygen-sensitive phosphorescent probe (Oxyphor PtG4) was injected into the tissues, and oxygen levels were monitored using a fiberoptic phosphorometer during UHDR irradiation with a 6 MeV electron linear accelerator (LINAC). Dose escalation experiments (10–40 Gy) were performed at a dose rate of 1300 Gy/s, and dose rate escalation experiments were conducted at a fixed dose of 40 Gy with dose rates ranging from 2 to 101 Gy/s.
Results: Radiation-induced change in tissue oxygenation (ΔpO_2) increased linearly with dose and correlated with baseline tissue oxygenation levels in the range of 0 – 30 mmHg. At higher baseline tissue oxygenation levels, such as those observed in muscle and brain, there was no corresponding increase in ΔpO_2. When we modulated dose rate, ΔpO_2 increased steeply up to ~ 20 Gy/s and plateaued thereafter. The relationship between ΔpO_2 and dose rate showcases the interplay between ROD and reoxygenation.
Conclusion: While UHDR irradiation induces measurable oxygen depletion in tissues, the observed changes in oxygenation levels do not support the hypothesis that ROD-induced radioresistance is responsible for the FLASH tissue-sparing effect at clinically relevant doses and dose rates. These findings highlight the need for further investigation into alternative mechanisms underlying the FLASH effect.

Introduction

FLASH radiotherapy (FLASH-RT) is an innovative approach in radiation oncology that employs ultra-high dose rates (UHDR, >100 Gy/s) reducing treatment duration to milliseconds or less, as opposed to minutes in conventional radiotherapy (CONV-RT, <10 Gy/min) protocols [1]. Such rapid dose delivery can elicit the FLASH effect, defined by reduced level of healthy tissue toxicity with equivalent anti-tumor effect in comparison with standard dose rates [2,3]. While there is considerable promise for FLASH-RT to improve the therapeutic ratio of radiotherapy practices [2], the precise mechanisms responsible for its differential effect on normal tissue versus tumor remains to be understood.

One of the proposed explanations for the FLASH effect involves rapid radiochemical oxygen depletion (ROD) as a result of irradiation at UHDR [4–7]. This hypothesis relies on the pivotal role that oxygen plays in amplifying the detrimental effects of ionizing radiation and its consumption through reactions with free radicals generated during irradiation. At sufficiently high dose and dose rates, the radiolytic oxygen consumption could surpass the rate of oxygen replenishment from the blood vessels, creating transient hypoxic conditions that might protect normal tissues. It was further suggested that in tumors that are already hypoxic, the potential gain in radioresistance would be minimal according to the classical concept of the oxygen enhancement ratio (OER) [8].

Clonogenic survival assays on bacterial and mammalian cells

* Corresponding author at: Department of Radiation Oncology, CHUV Lausanne, Switzerland.
E-mail address: Veljko.Grilj@chuv.ch (V. Grilj).
[1] Contributed equally to this manuscript.

https://doi.org/10.1016/j.radonc.2024.110539
Received 13 May 2024; Received in revised form 9 September 2024; Accepted 12 September 2024
Available online 17 September 2024

Table 1
Beam parameters used to for dose escalation experiments.

Dose (Gy)	DPP (Gy)	w (μs)	DR_p x 10^6 (Gy/s)	PRF (Hz)	N	DR_{av} (Gy/s)	Treatment time (ms)
10	10	1.8	5.56	100	1	5.56E+06	0.0018
20	10	1.8	5.56	100	2	2000	10
30	10	1.8	5.56	100	3	1500	20
40	10	1.8	5.56	100	4	1333	30

Table 2
Beam parameters used to investigate the correlation between the decrease in tissue oxygen concentration and the average dose rate.

Dose (Gy)	DPP (Gy)	w (μs)	DR_p x 10^5 (Gy/s)	PRF (Hz)	N	DR_{av} (Gy/s)	Treatment time (s)
40	0.4	1.8	2.22	250	100	101	0.4
40	0.4	1.8	2.22	100	100	40	1
40	0.4	1.8	2.22	50	100	20	2
40	0.4	1.8	2.22	20	100	8	5
40	0.4	1.8	2.22	10	100	4	10
40	0.4	1.8	2.22	5	100	2	20

conducted in the past provided the experimental basis showing that ROD induced by UHDR irradiation can indeed be protective when cells are irradiated at high doses in vitro [9–13]. In this case, the higher dose rate served to hinder the reoxygenation of cells through the diffusion of oxygen from the surrounding air during irradiation. However, this UHDR sparing effect was observed either at radiation doses that are much higher than those used in clinical radiotherapy, or if the cells were kept at very low oxygen pressure (<5 mmHg), a condition characteristic of hypoxic rather than normally oxygenated tissues. Hence, to assess the role of ROD in the sparing effect of FLASH-RT, it is crucial to directly monitor alterations in tissue oxygen levels during UHDR irradiation.

Recently, non-invasive *in vivo* oxygen measurements were proven feasible with the use of an optical oxygen sensing technique based on phosphorescence quenching [14–16]. The observed decrease in oxygen levels in the interstitial space and vasculature of the mouse leg muscle exposed to UHDR irradiation was insufficient to substantiate the hypothesis that ROD could cause radioresistance at the doses known to induce the FLASH sparing effect (e.g. 10 Gy). A similar result was obtained in the context of intracellular ROD measurements *in vitro* [15]. However, no comparable *in vivo* measurements are available in other normal tissues and tumors, where distinct tissue composition, initial oxygen levels, and blood perfusion potentially could influence ROD values. Moreover, previous *in vivo* studies investigated ROD used only dose rates above 90 Gy/s and were thus unable to examine the correlation between the dose rate dependencies of the ROD-caused change in tissue oxygen level and the magnitude of the FLASH sparing effect.

In this study, we applied the phosphorescence quenching method to assess and compare variations in oxygen levels induced by 10–40 Gy FLASH-RT (>1300 Gy/s) across different mouse tissues including skin, leg muscle, brain, and a subcutaneous (SQ) tumor model composed of human glioblastoma (U-87 MG). Crucially, we conducted irradiations using dose rates ranging from 2 to 101 Gy/s to decipher the relationship between ROD and reoxygenation during the irradiation process.

Materials and methods

Irradiation source and beam properties

The prototype 6 MeV electron LINAC Oriatron eRT6 (PMB, Alcen, France) [17] was used as a radiation source in this study. The LINAC generates electron pulses of 0.5–4 μs duration (w) at pulse repetition frequencies (PRF) ranging from 5-250 Hz. Apart from altering w, modification of the dose per pulse (DPP, the dose delivered by a single pulse) can be achieved by tuning the electron current and the source to surface distance (SSD). The combination of the number of pulses (n), DPP, and PRF determines the average dose rate (DR_{av}) according to the equation: $DR_{av} = D/t = (n*DPP*PRF)/(n-1)$, where D stands for the total dose and t stands for the irradiation time. For a single pulse irradiation, DR_{av} is equal to the pulse dose rate ($DR_p = DPP/w$). The beam parameters used in the present study are summarized in Table 1 and 2. For the dose escalation experiments (10–40 Gy), we utilized a DPP of 10 Gy and a PRF of 100 Hz to administer FLASH-RT to both normal and tumor tissues. The lowest DR_{av} was 1300 Gy/s, coupled with the longest irradiation time of 30 ms. Both values correspond to a 40 Gy dose delivered in 4 pulses. For exploring the correlation between the decrease in tissue oxygenation and DR_{av}, we lowered the DPP to 0.4 Gy and delivered 40 Gy in 100 pulses at different PRF ranging from 5-250 Hz. By doing so we were able to gradually change the DR_{av} ranging from 2 Gy/s to 100 Gy/s. The pulse duration, w, remained constant at 1.8 μs throughout all irradiations.

Oxygen probe

A water-soluble phosphorescent oxygen probe, Oxyphor PtG4, was utilized for sensing extracellular oxygen in tissues during irradiation [18,19]. Partial pressure of oxygen (pO_2) was determined using an OxyLED fiber optic phosphorometer (Oxygen Enterprises Ltd.) relying on the lifetime of phosphorescence emitted by Oxyphor molecules. Oxygen was measured at a frequency of ~ 7 measurements per second. Data acquisition followed the protocols described in [15].

Animal experiments

18 female Swiss Nude (NU(Ico)-Foxn1nu) mice (Charles River FR) aged either 10 or 24 weeks were used for SQ tumor and normal tissue experiments. 7 animals were used specifically for brain measurements and the remaining 11 were used for SQ tumor, skin, and muscle measurements (each animal was used for all three tissues). All animal experiments were approved by the Swiss ethics committees (VD3603) for animal experimentation and performed within institutional guidelines. All procedures were performed under anesthesia (Isoflurane, 3–4 % induction and 1–2 % maintenance) and euthanasia was performed at the end of the procedure.

Tumor model

U-87 MG (HTB-14, ATCC, Germany) human glioblastoma (GBM) were cultured in complete medium containing DMEM (Dulbecco's Modified Eagle Medium) + GlutaMAX (4.5 g/L D-Glucose, Pyruvate; 31966–021, Thermo Fisher Scientific) and supplemented with 10 % FBS (F7524, Sigma-Aldrich).

The U-87 MG SQ human GBM model consists of injecting 10^7 U-87 MG human GBM cells suspended in 100 μl PBS in the right flank of female Swiss Nude mice. Tumors were grown for 10 days (150–300 mm^3).

Injection of probe in preparation for measurements

For the direct injection of probe into SQ tumor, muscle, and skin: 50 μL of Oxyphor PtG4 probe (200 μM; Oxygen Enterprises Ltd., USA) was injected directly into each tissue of interest (subcutaneously, intramuscularly, and intratumorally) using a 29G insulin injector and then allowed to regain consciousness. A minimum of 2 h was given to ensure the spread and accumulation of the probe. SQ tumor, muscle, and skin pO_2 measurements were made in the same animal in each case.

For the direct injection of probe into brain: The Oxyphor probe (2 μL, 1.2 mM) was injected into the cerebral cortex according to the stereotactic coordinates table (coordinate AP=2mm; Lat = 1.5 mm; DV=1.8 mm from bregma) over a period of 5 min using an autoinjector, and then following sutures transferred to a recovery cage for observation. Around 8 h were given to ensure the spread of the probe. Animals used for the

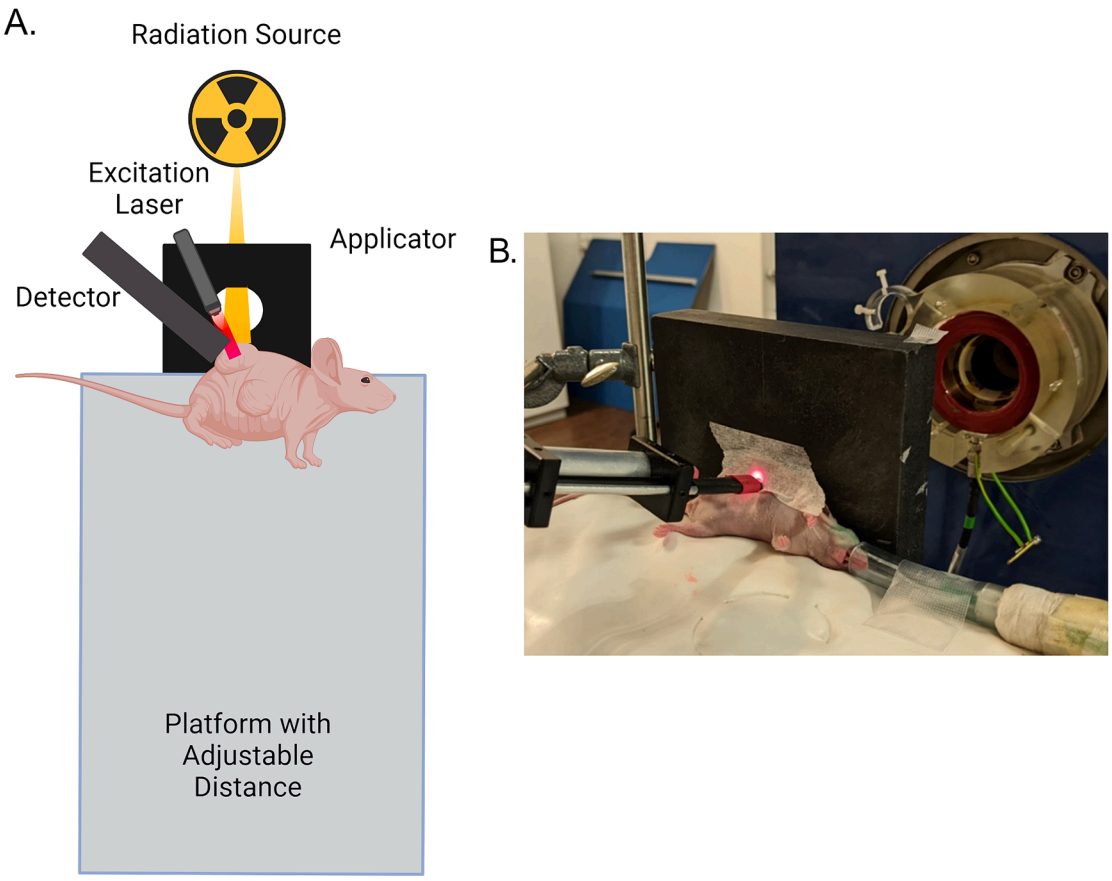

Fig. 1. Illustration (A) and photograph (B) of the irradiation set up with simultaneous pO_2 measurement. The animal, under Isoflurane anesthesia, was placed such that the tissue of interest could be easily positioned within the circular cutout of the graphite applicator. The tissue of interest was held in place with medical tape, the tip of the OxyLED detector fiber was positioned within millimeters of (but not in direct contact with) the tissue, and the signal-to-noise ratio was checked after the overhead lights were turned off. The phosphorometer computer was operated remotely from the command room outside the bunker.

brain pO_2 measurements were used uniquely for that purpose.

Mouse irradiation and oxygen measurements

The size of the radiation field was restricted by a graphite applicator of 1.7 cm in diameter. The applicator allowed for the delivery of the electron beam solely to the targeted tissue area, while the body was shielded from the beam. Whole brain irradiations were performed by laterally irradiating the mouse's head positioned immediately behind the applicator. The SQ tumors and normal skin underwent irradiation with a setup where the skin, either bearing the tumor or without it, was drawn from the flank and extended over the graphite applicator, which was positioned slightly above the mouse's body (as shown in Fig. 1). The hind leg thigh muscle was irradiated in a similar setup, with the leg pulled up from the mouse and placed in contact with the applicator.

Lateral profiles and percent depth dose distributions characteristic of the beam emerging from the applicator have been reported in [20]. The prescribed dose corresponded to the average dose from a 5 mm diameter circle around the beam isocenter on the surface of a solid water phantom (30 x 30 cm^2) positioned behind the applicator. Dose measurements on the surface of the phantom were carried out by GafChromic EBT3 films.

For oxygen measurements the laser diode served as the excitation light source, generating an excitation spot smaller than 200 μm in diameter on the tissue surface. Attention was given to aligning the laser spot with the isocenter of the radiation field shaped by the applicator. The phosphorescence signal emitted by the Oxyphor injected into tissue was gathered and conveyed back to the OxyLED phosphorometer using an optical fiber (4 mm diameter). The tip of the fiber was positioned a few millimeters away from the surface of the tissue and directed towards the illuminated laser spot. All measurements were performed under anesthesia, and the animal was euthanized at the end of the experiment before awakening by cervical dislocation followed by exsanguination. The sequence of the radiation conditions used (e.g. 10 Gy – 20 Gy – 30 Gy – 40 Gy or 250 Hz – 100 Hz – 50 Hz – 20 Hz – 10 Hz) was randomized for each tissue-animal combination to ensure that the data were consistent and not due to a specific sequence.

Statistical methods

Single data points representing ΔpO_2 were calculated by subtraction of pO_2 value averaged over 5 s before the irradiation and the minimum pO_2 value reached immediately after the beam was turned off. Relative ΔpO_2 readings were calculated by normalizing data points to the maximum DR_{av} data point (for each animal/tissue combination). Where aggregate data is shown it is presented as a mean or mean ± SEM. All plots were generated in GraphPad Prism 9/10.

Results

Using our setup, we measured interstitial pO_2 continuously before, during, and following FLASH-RT in healthy and malignant tissues. First, we performed the dose escalation experiment using single-pulse FLASH mode for the eRT6: DPP of 10 Gy, w of 1.8 μs and PRF of 100 Hz (see Table 1). We found that local tissue pO_2 depletion (denoted by ΔpO_2 and defined in Fig. 2A) increased in a dose-dependent manner – with a simple linear relationship between dose delivered and mmHg of pO_2 depleted for each of the different tissues of interest (Fig. 2). We were not able to detect any ΔpO_2 when using the conventional (~0.1 Gy/s) dose rate. We define the calculated slope of these linear relationships as the

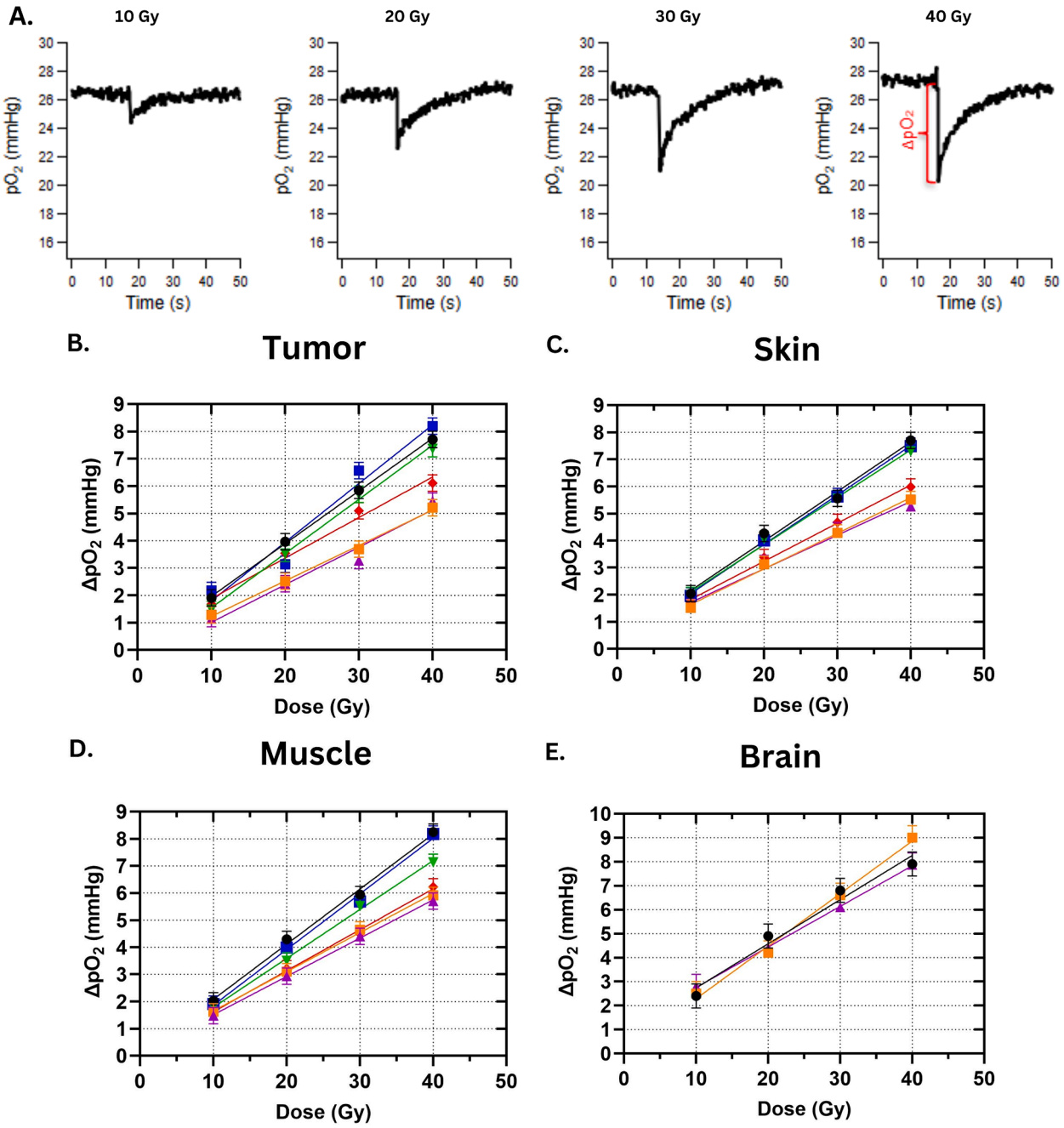

Fig. 2. UHDR RT depletion of interstitial oxygen *in vivo* increases linearly with dose between 10 and 40 Gy. (A) Representative measurements (in skin) for each dose in a dose escalation experiment. Definition of ΔpO_2 is indicated for a dose of 40 Gy. Calculated measurements of ΔpO_2 plotted against the delivered dose for each tissue: SQ tumor **(B)**, skin **(C)**, muscle **(D)**, and brain **(E)**. Each color represents a different animal. Values are presented as mean ± SEM.

Table 3
G-values for each animal/tissue calculated from the dose escalation ΔpO_2 data. Skin, Muscle, and SQ Tumor were measured in the same animals, for the Brain measurements separate animals were used.

	Skin	Muscle	Brain*	SQ Tumor
Average	0.15 ± 0.03	0.17 ± 0.03	0.19 ± 0.03	0.17 ± 0.03
Mouse 1	0.18 ± 0.01	0.203 ± 0.009	0.18 ± 0.02	0.198 ± 0.007
Mouse 2	0.131 ± 0.007	0.144 ± 0.004	0.22 ± 0.01	0.14 ± 0.02
Mouse 3	0.12 ± 0.01	0.141 ± 0.003	0.169 ± 0.002	0.130 ± 0.005
Mouse 4	0.175 ± 0.08	0.180 ± 0.005		0.193 ± 0.003
Mouse 5	0.141 ± 0.06	0.151 ± 0.006		0.15 ± 0.01
Mouse 6	0.181 ± 0.06	0.21 ± 0.01		0.21 ± 0.03

ROD G-value. The ROD G-values determined for all tissues of interest can be found in Table 3. They fell within the range of 0.13 to 0.21 mmHg/Gy for SQ tumors, 0.12 to 0.18 mmHg/Gy for skin, 0.14 to 0.21 mmHg/Gy for muscle and 0.17 to 0.22 mmHg/Gy for brain.

We observed a positive correlation between the measured ΔpO_2 and the baseline pO_2 of irradiated tissue – up to ~ 32 mmHg – at each given dose, shown in Fig. 3. This relationship was strong in tissues with lower baseline pO_2 (SQ tumor and skin; Fig. 3A-B), but the slope decreased to nearly zero in tissues with higher baseline pO_2 (muscle and brain; Fig. 3C-D). We observe the flattening of the trend above ~ 32 mmHg baseline pO_2 clearly in Fig. 3E where we plotted together the G-values determined for all doses and tissues represented in Fig. 3A-D.

In subsequent experiments, we used a fixed dose (40 Gy) and

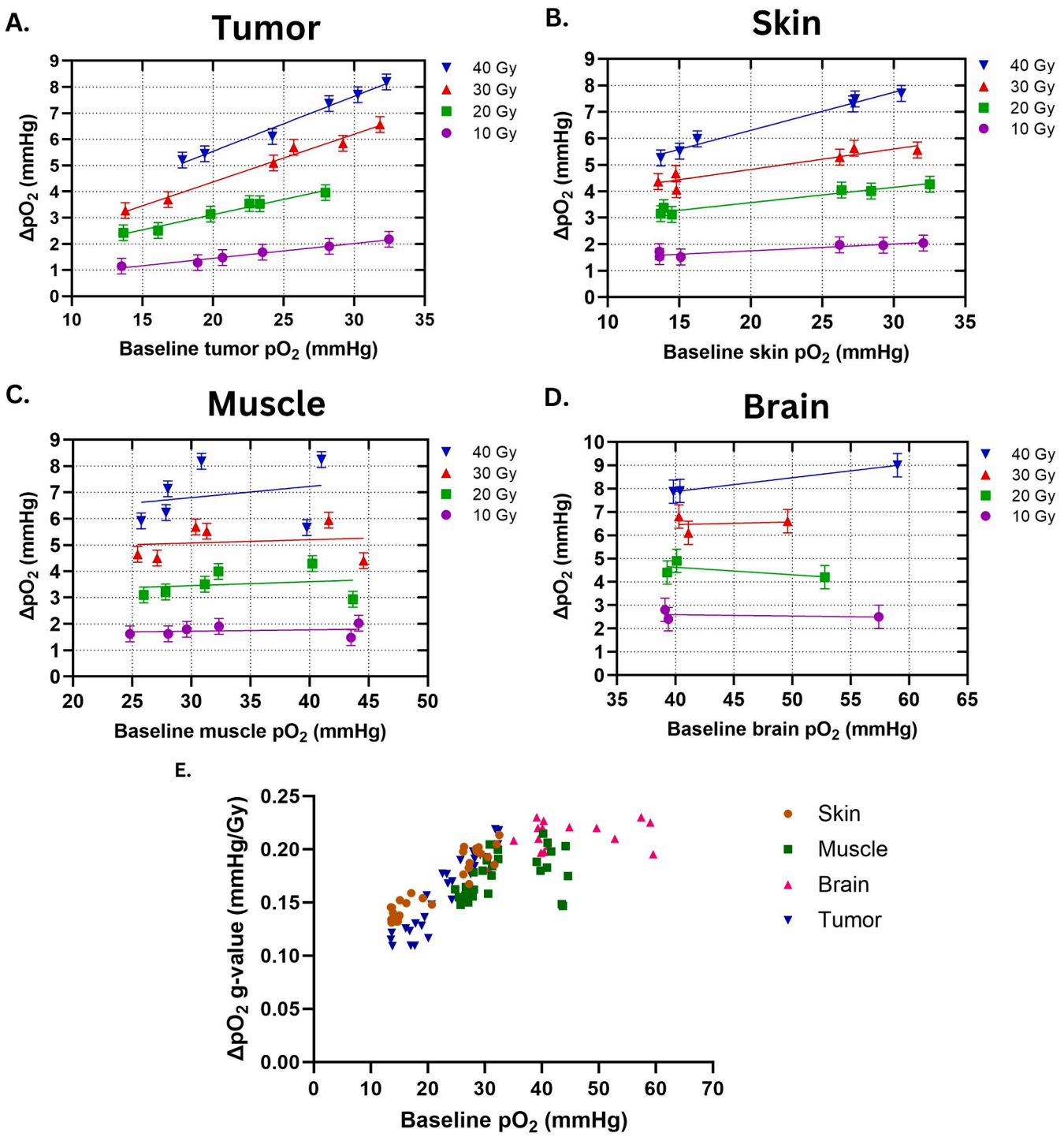

Fig. 3. The bimodal (linear at lower baseline pO_2, plateau above 32 mmHg pO_2) relationship between ΔpO_2 resulting from UHDR RT and baseline tissue pO_2. Calculated measurements of ΔpO_2 plotted against the baseline pO_2 level for each tissue: SQ tumor **(A),** skin **(B),** muscle **(C),** and brain **(D).** Values are presented as mean ± SEM. **(E)** ROD G-Values plotted against the baseline pO_2 level. Each icon represents the ROD value calculated from an individual measurement.

modulated the treatment time and consequently the DR_{av}. We decreased the DPP to 0.4 Gy/pulse and varied the PRF from 5 Hz to 250 Hz (the lower and upper limits of the instrument, respectively). Using these settings, we measured the ΔpO_2 for a range of time-averaged dose rates (DR_{AV}) from 2 Gy/s to 101 Gy/s (sample measurements shown in Fig. 4A). In these experiments, ΔpO_2 values were a function of both ROD and reoxygenation, as the treatment time for the lowest dose rate increased to 20 s. The observed relationship between ΔpO_2 and dose rate was qualitatively similar for all tissues and animals, revealing the steep increase in ΔpO_2 at low dose rates followed by flattening of the curve at $\geq$ 20 Gy/s (Fig. 4B-E).

For further analysis, we normalized ΔpO_2 values individually for each animal and tissue to the maximum ΔpO_2 value recorded for that animal (at 101 Gy/s), assuming that at 101 Gy/s the contribution of reoxygenation is negligible. To justify this assumption, we compared ΔpO_2 values for 101 Gy/s with those obtained for the FLASH beam delivered at more than 1300 Gy/s (**Fig. S1**). This normalization significantly reduced the discrepancies between the curves belonging to the

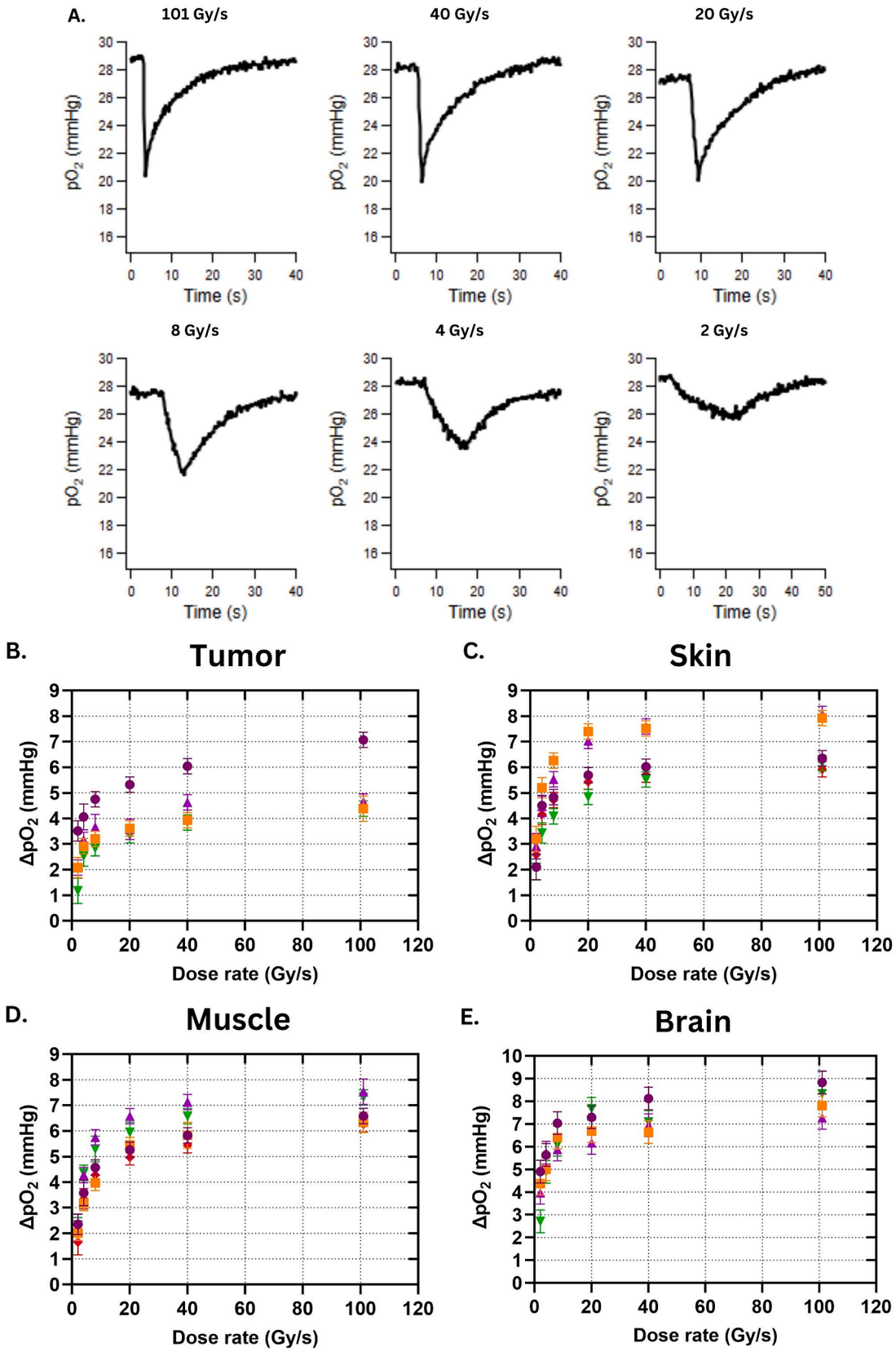

Fig. 4. A consistent trend observed between the change in absolute tissue oxygen level (ΔpO_2) and DR_{AV} for all measured tissues. (A) Representative measurements (in skin) for each dose rate in the dose rate escalation experiment. Calculated measurements of ΔpO_2 plotted against the delivered dose rate for each tissue: SQ tumor **(B)**, skin **(C)**, muscle **(D)**, and brain **(E)**. Each color represents a different animal. Values are presented as mean ± SEM.

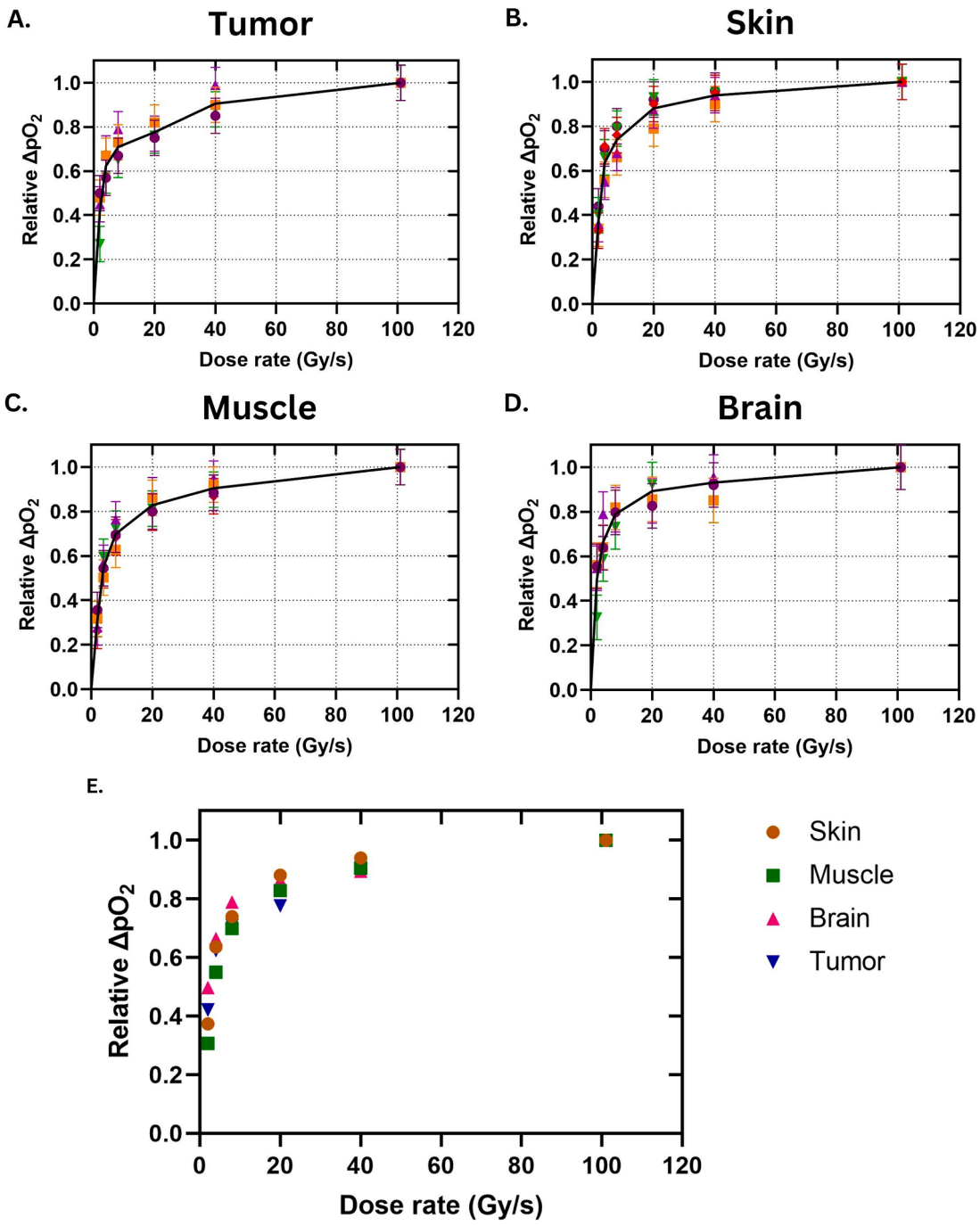

Fig. 5. An identical trend observed between relative ΔpO_2 and DR_{AV} for all measured tissues. Calculated measurements of relative ΔpO_2 plotted against the dose rate for each tissue: SQ tumor **(A)**, skin **(B)**, muscle **(C)**, and brain **(D)**. Each color represents a different animal. Values are presented as mean ± SEM. Black lines connect mean relative ΔpO_2 values to indicate the trend. **(E)** Relative ΔpO_2 plotted against the dose rate. Each point represents the mean relative ΔpO_2 value calculated for each tissue at that dose rate (error bars were omitted to allow for easier intercomparison of relative ΔpO_2 for different tissues).

same tissue but different animals (Fig. 5 **A-D**) indicating that the proportion of ΔpO_2's at lower dose rates relative to ΔpO_2's at the highest dose rate applied (101 Gy/s) is quite stable. Moreover, when plotted together, the average relative ΔpO_2 values (from the normalization described earlier) determined for all tissues revealed nearly the same dependence on DR_{av} (Fig. 5E).

Discussion

Using an Oxyphor oxygen probe and the OxyLED phosphorometer, we have performed *in vivo* real-time ROD measurements before, during, and after FLASH-RT *in multiple tissues including malignant tissue* at different baseline pO_2. We highlighted a novel relationship between relative ROD and DR_{av}. Furthermore, we have presented the first measurement of *in vivo* real-time ROD during UHDR RT in the brain – a late-responding (to irradiation) tissue with the most comprehensive FLASH-RT tissue sparing profile to date.

First, we confirmed that a measurable decrease in tissue pO_2 takes place during UHDR RT, but not during CONV-RT. This result is consistent with previous reports [14–16] and constitutes an important observation – any decrease in tissue pO_2 is indicative that ROD at ultra-high dose rates is able to overwhelm the rate of reoxygenation from the

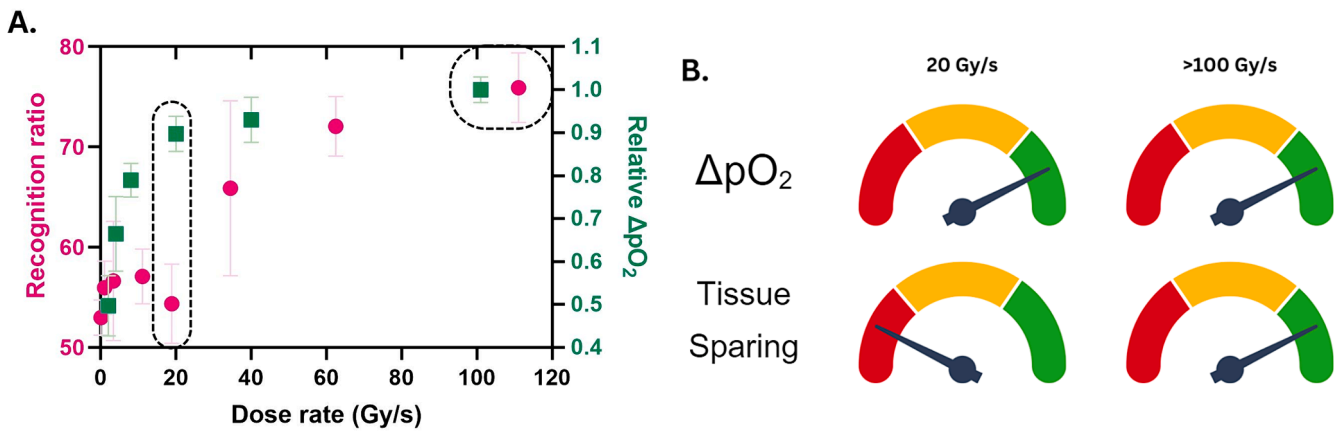

Fig. 6. Relative change in brain oxygenation (relative ΔpO_2) following RT in mouse brain and Recognition Ratio [20] versus Average Dose Rate (Gy/s). (A) Relative ΔpO_2 measurements (green) and previously published novel object recognition ratio (higher values indicating better protection, pink) plotted against the reported dose rate. Dashed black ovals indicate the data points used for part (B). (B) Illustration indicating difference in change of tissue oxygenation (ΔpO_2) versus tissue sparing at ~ 20 Gy/s and at > 100 Gy/s based on data from (A). (For interpretation of the references to color in this figure legend, the reader is referred to the web version of this article.). (For interpretation of the references to color in this figure legend, the reader is referred to the web version of this article.)

blood, causing a transient local depression in pO_2 within the radiation field. However, in our study, we observed similar ROD g-values across the board in both SQ tumor and non-malignant tissues, so it would be difficult to explain the FLASH effect with this observation using the hypothesis proposed by Spitz et al. [4]. Instead, the calculated G-values further support that the amount of oxygen depleted is not sufficient to cause radiobiological hypoxia (i.e. protect healthy tissue) at the doses that were used to elicit the FLASH effect (<40 Gy) [20–24], echoing a number of the previous studies [14–16].

Furthermore, the mean baseline pO_2 readings in our SQ tumor model were not universally hypoxic and showed considerable variability. In fact, the baseline pO_2 registered in the mouse flank skin (~13–32 mmHg) had a similar range as in the U-87 MG GBM SQ tumor (~14–33 mmHg). FLASH dose modifying factor for skin has previously been shown to be 1.44–1.58 [24], while in this exact tumor model, we have shown equivalent efficacy of FLASH- and CONV-RT at *iso*-dose [25]. Such divergent effects of FLASH-RT on normal skin and U-87 MG GBM SQ tumor cannot be explained by ROD alone, considering that both the ROD g-values and the baseline pO_2 values for skin and the SQ tumor were similar.

We took our examination of *in vivo* FLASH ROD further by making additional observations and relating defined variables to the measured ROD. First, we showed that ΔpO_2 scales linearly with the delivered dose up to 40 Gy (using single-pulse 10 Gy DPP beam setup). The slopes of these linear trends give the ROD G-values. Cao et al. also observed a linear relationship [14], but in contrast the ΔpO_2 values differed significantly between their flank tumors and the contralateral leg tissue. However, this discrepancy can be explained by our second observation, mirroring results of some previous studies [15,16], namely that ΔpO_2 values also scale with baseline tissue pO_2. Given the notably lower baseline pO_2 in Cao et al.'s tumor model (MDA-MB-237, ~9–14 mmHg pO_2) compared to our U-87 MG GBM model (~14–33 mmHg pO2), it is reasonable to anticipate lower ΔpO_2 values in their case. Moreover, their normal tissue measurement was likely most analogous to our muscle pO_2 sampling, whose baseline pO_2 was consistently higher than our SQ tumor measurements. This combination of factors informed their result of significantly different G-values for tumors and normal tissue – a result we could not confirm in our study.

Absolute ΔpO_2 plotted against DR_{av} for each tissue type reveal a correlation between the two variables, a consequence of the dueling factors of ROD and tissue reoxygenation. In fact, for each individual animal a smooth curve could be drawn with a sharp increase up to about 20 Gy/s and then flattening from 20 Gy/s to 101 Gy/s. It is worth noting that, based on in vitro measurements of ROD G-values in sealed samples containing various media [26,27], ROD G-values in tissue may inherently depend on DR_{av}. This dependence would influence the measured ΔpO2 values, but it cannot be directly assessed *in vivo* because it is confounded by oxygen recovery during irradiation. Having made these observations and found that all of the ΔpO_2 curves were qualitatively similar, we normalized the measured absolute ΔpO_2 values to the maximum ΔpO_2 achieved for that tissue/animal combination at 101 Gy/s (250 Hz PRF), thus deriving a value referred to as relative ΔpO_2. We justified this by showing that irradiations at 101 Gy/s resulted in ΔpO_2 values similar to those resulting from FLASH irradiations at rates higher than 1300 Gy/s (**Fig. S1**). Following normalization, we plotted the relationship between relative ΔpO_2 and DR_{av} demonstrating that the observed trend was consistent, not just for each tissue, but among all healthy and cancerous mouse tissues measured. To our knowledge, this is the first time this important relationship between DR_{av} and ΔpO_2 in tissue has been shown.

The relative ΔpO_2 values enable us to predict the overall tissue pO_2 change anticipated at any dose rate as a proportion of the pO_2 alteration at 101 Gy/s. The significance of this arises from the previous findings of Montay-Gruel et al., demonstrating that the maximum measurable preservation of normal brain tissue occurred at 100 Gy/s, without additional benefits detected beyond this dose rate using this model and endpoint [20]. In fact, we intentionally lowered the dose rate from 100 Gy/s down to 2 Gy/s to span the range across which the cognitive sparing in the brain becomes completely undetectable [20]. In Fig. 6A, we present a direct comparison between the dose rate dependencies of cognitive brain function [20], assessed by the novel object recognition ratio, and the relative ΔpO_2 measurements acquired from our mouse brain irradiations. The data clearly show that long-term (late responding) tissue sparing in the brain does not track directly with the decrease in brain pO_2 as a result of UHDR RT. While UHDR RT achieved ~ 90 % of maximum local oxygen depletion at 20 Gy/s, there was close to zero cognitive sparing effect observed at this dose rate (Fig. 6B). This result shows that protective hypoxia from ROD is not the cause of the FLASH tissue sparing effect.

Overall, this study offers the most comprehensive collection of tissues, doses, and dose rates examined systematically in the context of *in vivo* ROD measurements. We have presented the first results for ΔpO_2 during UHDR RT in the mouse brain and determined ROD G-values for four different tissues (including GBM SQ tumor). The study was done in female mice as it is our model of reference [20,28–34]. Further investigation into the effects of UHDR radiation in males is warranted, as suggested by Tavakkoli et al. [35]. Oxyphor probes have been widely used to quantify oxygenation levels in many biological applications and

have been recently used to quantify oxygen depletion during radiation treatment [14–16,36–38]. Oxyphor molecules do not diffuse across cellular membranes, and hence our tissue measurements reported in this work are limited to the extracellular space. However, a recent study has shown that intracellular ROD by FLASH is very close to extracellular ROD measured *in vitro* [26]. We also acknowledge that there is just one tumor type measured in this study and there are plans to expand on this work. Ultimately, given the incontrovertible importance of oxygen (but arguably not the ROD-induced radioresistance) to the FLASH effect, these novel measurements and observed relationships are necessary to propel the field forward towards a better understanding of oxygen dynamics during FLASH-RT and the reoxygenation process occurring in parallel with ROD.

CRediT authorship contribution statement

Veljko Grilj: Writing – review & editing, Writing – original draft, Visualization, Validation, Supervision, Methodology, Investigation, Formal analysis, Data curation, Conceptualization. **Ron J. Leavitt:** Writing – review & editing, Writing – original draft, Visualization, Validation, Methodology, Investigation, Data curation, Conceptualization. **Mirna El Khatib:** Writing – review & editing, Writing – original draft, Validation, Methodology, Investigation. **Ryan Paisley:** Writing – review & editing, Methodology, Investigation. **Javier Franco-Perez:** . **Benoit Petit:** . **Paola Ballesteros-Zebadua:** Writing – review & editing, Writing – original draft, Methodology, Investigation, Conceptualization. **Marie-Catherine Vozenin:** Writing – review & editing, Validation, Supervision, Resources, Funding acquisition, Conceptualization.

Declaration of competing interest

The authors declare the following financial interests/personal relationships which may be considered as potential competing interests: Marie-Catherine Vozenin reports financial support was provided by Swiss National Science Foundation. Marie-Catherine Vozenin reports financial support was provided by National Institutes of Health. Mirna El Khatib reports financial support was provided by National Institutes of Health. Paola Ballesteros-Zebadua reports financial support was provided by Swiss National Science Foundation. If there are other authors, they declare that they have no known competing financial interests or personal relationships that could have appeared to influence the work reported in this paper.

Acknowledgments

The authors thank Prs J Bourhis and Prof F Bochud for their support, and Prof S Vinogradov for expert advice. We also thank the animal facility at Epalinges.

Funding was provided by Swiss National Science Foundation grant MAGIC - FNS CRS II5_186369 (to MCV supporting RJL, VG, RP), National Institutes of Health grant P01CA244091-01 (to MCV supporting VG), Swiss National Science Foundation grant Spirit IZSTZ0_198747/1 (to MCV and PBZ supporting JFP), and National Institutes of Health grant HL145092 (to MEK).

Appendix A. Supplementary data

Supplementary data to this article can be found online at https://doi.org/10.1016/j.radonc.2024.110539.

References

[1] Gao Y, Liu R, Chang C-W, Charyyev S, Zhou J, Bradley JD, et al. A potential revolution in cancer treatment: A topical review of FLASH radiotherapy. J Appl Clin Med Phys 2022;23:e13790.

[2] Vozenin M-C, Bourhis J, Durante M. Towards clinical translation of FLASH radiotherapy. Nat Rev Clin Oncol 2022;19:791–803. https://doi.org/10.1038/s41571-022-00697-z.

[3] Limoli CL, Vozenin M-C. Reinventing radiobiology in the light of FLASH radiotherapy. Ann Rev Cancer Biol 2023;7:1–21. https://doi.org/10.1146/annurev-cancerbio-061421-022217.

[4] Spitz DR, Buettner GR, Petronek MS, St-Aubin JJ, Flynn RT, Waldron TJ, et al. An integrated physico-chemical approach for explaining the differential impact of FLASH versus conventional dose rate irradiation on cancer and normal tissue responses. Radiother Oncol 2019;139:23–7. https://doi.org/10.1016/j.radonc.2019.03.028.

[5] Pratx G, Kapp DS. Ultra-high-dose-rate FLASH irradiation may spare hypoxic stem cell niches in normal tissues. Int J Radiation Oncol*Biol*Phys 2019;105:190–2. DOI: 10.1016/j.ijrobp.2019.05.030.

[6] Petersson K. FLASH radiotherapy: What, how and why? Res Outreach 2020;2020:66–9. https://doi.org/10.32907/RO-117-6669.

[7] Rothwell BC, Kirkby NF, Merchant MJ, Chadwick AL, Lowe M, Mackay RI, et al. Determining the parameter space for effective oxygen depletion for FLASH radiation therapy. Phys Med Biol 2021;66:055020. https://doi.org/10.1088/1361-6560/abe2ea.

[8] Hall EJ, Cox JD. Chapter 1 - Physical and Biologic Basis of Radiation Therapy. In: Cox JD, Ang KK, editors. Radiation Oncology. Ninth Edition. Philadelphia: Mosby; 2010. p. 3–49.

[9] Epp ER. Recent developments in fundamental radiobiology. Cancer 1968;22:802–8. https://doi.org/10.1002/1097-0142(196810)22:4<802::AID-CNCR2820220417>3.0.CO;2-A.

[10] Nias AHW, Swallow AJ, Keene JP, Hodgson BW. Effects of pulses of radiation on the survival of mammalian cells. Br J Radiol 1969;42:553. https://doi.org/10.1259/0007-1285-42-499-553-b.

[11] Epp ER, Weiss H, Djordjevic B, Santomasso A. The radiosensitivity of cultured mammalian cells exposed to single high intensity pulses of electrons in various concentrations of oxygen. Radiat Res 1972;52:324–32. https://doi.org/10.2307/3573572.

[12] Weiss H, Epp ER, Heslin JM, Ling CC, Santomasso A. Oxygen depletion in cells irradiated at ultra-high dose-rates and at conventional dose-rates. Int J Radiat Biol Relat Stud Phys Chem Med 1974;26:17–29. https://doi.org/10.1080/09553007414550901.

[13] Michaels HB, Epp ER, Ling CC, Peterson EC. Oxygen sensitization of CHO cells at ultrahigh dose rates: prelude to oxygen diffusion studies. Radiat Res 1978;76:510–21. https://doi.org/10.2307/3574800.

[14] Cao X, Zhang R, Esipova TV, Allu SR, Ashraf R, Rahman M, et al. Quantification of oxygen depletion during FLASH irradiation in vitro and in vivo. Int J Radiation Oncol*Biol*Phys 2021;111:240–8. DOI: 10.1016/j.ijrobp.2021.03.056.

[15] El Khatib M, Van Slyke AL, Velalopoulou A, Kim MM, Shoniyozov K, Allu SR, et al. Ultrafast tracking of oxygen dynamics during proton FLASH. Int J Radiation Oncol*Biol*Phys 2022;113:624–34. DOI: 10.1016/j.ijrobp.2022.03.016.

[16] Van Slyke AL, El Khatib M, Velalopoulou A, Diffenderfer E, Shoniyozov K, Kim MM, et al. Oxygen monitoring in model solutions and in vivo in mice during proton irradiation at conventional and FLASH dose rates. Radiat Res 2022;198:181–9. https://doi.org/10.1667/RADE-21-00232.1.

[17] Jaccard M, Durán MT, Petersson K, Germond J-F, Liger P, Vozenin M-C, et al. High dose-per-pulse electron beam dosimetry: Commissioning of the Oriatron eRT6 prototype linear accelerator for preclinical use. Med Phys 2018;45:863–74. https://doi.org/10.1002/mp.12713.

[18] Lebedev AY, Cheprakov AV, Sakadžić S, Boas DA, Wilson DF, Vinogradov SA. Dendritic phosphorescent probes for oxygen imaging in biological systems. ACS Appl Mater Interfaces 2009;1:1292–304. https://doi.org/10.1021/am9001698.

[19] Esipova TV, Barrett MJP, Erlebach E, Masunov AE, Weber B, Vinogradov SA. Oxyphor 2P: A high-performance probe for deep-tissue longitudinal oxygen imaging. Cell Metab 2019;29:736–744.e7. https://doi.org/10.1016/j.cmet.2018.12.022.

[20] Montay-Gruel P, Petersson K, Jaccard M, Boivin G, Germond JF, Petit B, et al. Irradiation in a flash: Unique sparing of memory in mice after whole brain irradiation with dose rates above 100Gy/s. Radiother Oncol 2017;124:365–9. https://doi.org/10.1016/j.radonc.2017.05.003.

[21] Favaudon V, Caplier L, Monceau V, Pouzoulet F, Sayarath M, Fouillade C, et al. Ultrahigh dose-rate FLASH irradiation increases the differential response between normal and tumor tissue in mice. Sci Transl Med 2014;6:245ra93. DOI: 10.1126/scitranslmed.3008973.

[22] Levy K, Natarajan S, Wang J, Chow S, Eggold JT, Loo PE, et al. Abdominal FLASH irradiation reduces radiation-induced gastrointestinal toxicity for the treatment of ovarian cancer in mice. Sci Rep 2020;10:21600. https://doi.org/10.1038/s41598-020-78017-7.

[23] Soto LA, Casey KM, Wang J, Blaney A, Manjappa R, Breitkreutz D, et al. FLASH irradiation results in reduced severe skin toxicity compared to conventional-dose-rate irradiation. Radiat Res 2020. https://doi.org/10.1667/RADE-20-00090.

[24] Singers Sørensen B, Krzysztof Sitarz M, Ankjærgaard C, Johansen J, Andersen CE, Kanouta E, et al. *In vivo* validation and tissue sparing factor for acute damage of pencil beam scanning proton FLASH. Radiother Oncol 2022;167:109–15. https://doi.org/10.1016/j.radonc.2021.12.022.

[25] Leavitt RJ, Almeida A, Grilj V, Montay-Gruel P, Godfroid C, Petit B, et al. Acute hypoxia does not alter tumor sensitivity to FLASH radiotherapy. Int J Radiation Oncol, Biol, Phys 2024;0. DOI: 10.1016/j.ijrobp.2024.02.015.

[26] Grilj V, Paisley R, Sprengers K, Geyer WR, Bailat C, Bochud F, et al. Average dose rate is the primary determinant of lipid peroxidation in liposome membranes

exposed to pulsed electron FLASH beam. Radiat Phys Chem 2024;222:111887. https://doi.org/10.1016/j.radphyschem.2024.111887.
[27] Sunnerberg JP, Zhang R, Gladstone DJ, Swartz HM, Gui Jiang, Pogue BW. Mean dose rate in ultra-high dose rate electron irradiation is a significant predictor for O_2 consumption and H_2O_2 yield. Physics in Medicine&Biology 2023; 68:165014. DOI: 10.1088/1361-6560/ace877.
[28] Montay-Gruel P, Acharya MM, Petersson K, Alikhani L, Yakkala C, Allen BD, et al. Long- term neurocognitive benefits of FLASH radiotherapy driven by reduced reactive oxygen species. PNAS 2019;116:10943–51. https://doi.org/10.1073/pnas.1901777116.
[29] Montay-Gruel P, Markarian M, Allen BD, Baddour JD, Giedzinski E, Jorge PG, et al. Ultra- high-dose-rate FLASH irradiation limits reactive gliosis in the brain. Radiat Res 2020;194:636–45. https://doi.org/10.1667/RADE-20-00067.1.
[30] Montay-Gruel P, Acharya MM, Gonçalves Jorge P, Petit B, Petridis IG, Fuchs P, et al. Hypofractionated FLASH-RT as an effective treatment against glioblastoma that reduces neurocognitive side effects in mice. Clin Cancer Res 2021;27:775–84. https://doi.org/10.1158/1078-0432.CCR-20-0894.
[31] Allen BD, Acharya MM, Montay-Gruel P, Jorge PG, Bailat C, Petit B, et al. Maintenance of tight junction integrity in the absence of vascular dilation in the brain of mice exposed to ultra-high-dose-rate FLASH irradiation. Radiat Res 2020; 194:625–35. https://doi.org/10.1667/RADE-20-00060.1.
[32] Allen BD, Alaghband Y, Kramár EA, Ru N, Petit B, Grilj V, et al. Elucidating the neurological mechanism of the FLASH effect in juvenile mice exposed to hypofractionated radiotherapy. Neuro Oncol 2023;25:927–39. https://doi.org/10.1093/neuonc/noac248.
[33] Alaghband Y, Allen BD, Kramár EA, Zhang R, Drayson OGG, Ru N, et al. Uncovering the protective neurologic mechanisms of hypofractionated FLASH radiotherapy. Cancer Res Commun 2023;3:725–37. https://doi.org/10.1158/2767-9764.CRC-23-0117.
[34] Alaghband Y, Cheeks SN, Allen BD, Montay-Gruel P, Doan NL, Petit B, et al. Neuroprotection of radiosensitive juvenile mice by ultra-high dose rate FLASH irradiation. Cancers (Basel) 2020;12:1671. https://doi.org/10.3390/cancers12061671.
[35] Tavakkoli AD, Clark MA, Kheirollah A, Sloop AM, Soderholm HE, Daniel NJ, et al. Anesthetic oxygen use and sex are critical factors in the FLASH sparing effect. Adv Radiation Oncol 2024;9:101492. https://doi.org/10.1016/j.adro.2024.101492.
[36] El Khatib M, Motlagh AO, Beyer JN, Troxler T, Allu SR, Sun Q, et al. Direct measurements of FLASH-induced changes in intracellular oxygenation. Int J Radiation Oncol*Biol*Phys 2024;118:781–9. DOI: 10.1016/j.ijrobp.2023.09.019.
[37] Cao X, Rao Allu S, Jiang S, Jia M, Gunn JR, Yao C, et al. Tissue pO2 distributions in xenograft tumors dynamically imaged by Cherenkov-excited phosphorescence during fractionated radiation therapy. Nat Commun 2020;11:573. https://doi.org/10.1038/s41467-020-14415-9.
[38] Cao X, Allu SR, Jiang S, Gunn B Jason R, Yao P Cuiping, Xin P Jing, et al. High-resolution pO2 imaging improves quantification of the hypoxic fraction in tumors during radiation therapy. Int J Radiation Oncol*Biol*Phys 2021;109:603–13. DOI: 10.1016/j.ijrobp.2020.09.046.